Electron and ion dynamics in graphene and graphane fragments subjected to high-intensity laser pulses

Sergiy Bubin and Kálmán Varga

Phys. Rev. B **85**, 205441 — Published 24 May 2012

DOI: 10.1103/PhysRevB.85.205441

Electron and ion dynamics in graphene and graphane fragments subjected to high-intensity laser pulses

Sergiy Bubin and Kálmán Varga
Department of Physics and Astronomy, Vanderbilt University, Nashville, Tennessee 37235, USA

In the framework of real-time real-space time-dependent density functional theory complemented with Ehrenfest molecular dynamics we have studied the response of small graphene and graphane fragments to intense femtosecond laser pulses. In particular, we have investigated how the response changes when laser pulses of different frequency (near IR, visible, and UV). The results of our simulations show that graphene has very high immediate (i.e. within laser pulse duration) damage threshold. They also suggest that, similarly to the case of other hydrogenated surfaces, it should be possible to selectively desorb hydrogens from graphane without destroying the underlying carbon structure provided that the laser pulse parameters are properly chosen.

PACS numbers: 33.80.Rv,78.67.Wj,79.70.+q

I. INTRODUCTION

The understanding of the interaction of intense, ultrashort laser pulses and graphene is a key prerequisite for both laser patterning and cleaning, as well as for applications of graphene in optical devices. Laser-induced bond breaking, defect formation, and damage mechanisms have been intensively investigated since the advent of high power laser pulses[1,2]. Unlike their long-pulse counterparts, material processing with ultrashort-pulse lasers have negligible heat diffusion effects, minimal plasma absorption, and require smaller laser fluences for processing, making them ideal for achieving high spatial resolution[3,4]. The effect of the laser pulse on the material strongly depends on the absorbed energy, which is determined by the material properties, as well as on the strength, intensity, shape, and duration of the pulse. The energy transport during the interaction of short laser pulses and materials is usually divided into two steps: (1) excitation of the electrons by the laser electromagnetic field whose potential is comparable or higher than the electrostatic potential that governs the chemical bonds and (2) distribution of the absorbed energy to the ionic degrees of freedom. The process in the first step is faster, starting immediately with the laser pulse. The second step is somewhat delayed in time.

Various aspects of the interaction of light and graphene have been experimentally investigated, including the study of laser induced band gaps[5–7], the response of graphene to femtosecond high-intensity laser irradiation[8,9], laser direct growth of graphene[10], and the laser-induced disassembly of a graphene single crystal into a nanocrystalline network[11]. Theoretical works investigating the interaction of carbon-based nanostructures include ab initio studies of photoexfoliation of graphene from graphite[12] and graphene production by laser shot on graphene oxide[13].

With its two-dimensional geometry, graphene is a novel testing ground for investigation of laser irradiation effect on planar nanostructures. Unlike surfaces, where the laser field interacts with multiple layers of atomic planes, in graphene a single layer has to withstand the deposited energy. It is therefore an interesting question to what extent the planar structure of graphene affects the thresholds for its nonlinear optical response.

In this work we will carry out first-principles time-dependent simulations of the interaction of intense short laser pulses with graphene and graphane using time-dependent density functional calculations complemented with Ehrenfest molecular dynamics. First principles simulations are indispensable tools to gain insight into the physical mechanisms behind the highly nonequilibrium and nonlinear processes, such as laser-induced structural deformation of graphene. The results of the study enhance our understanding of the dynamics of electrons and atoms in two dimensional materials. The theoretical and computational framework used in the present study has been successfully used in connection with laser-assisted desorption of hydrogen atoms from H-Si(111) surface[14,15].

II. COMPUTATIONAL METHOD

Density functional theory (DFT)[16,17] is now well established as one of the most capable methods for computing electronic ground state properties. In its original formulation, DFT only applies to the electronic ground state. Runge and Gross[18] generalized DFT to time-dependent systems. According to the Runge-Gross theorem, for any given initial state of a many-electron system, a time-dependent potential acting on it is uniquely determined by the subsequent time evolution of the one-electron density. Using this theorem, it is possible to formally establish a time-dependent Kohn-Sham (KS) equation from which various one-particle properties of the system can be obtained as functions of time. The resulting theoretical framework is usually referred to as time dependent density functional theory (TDDFT)[19].

The electron dynamics in our simulations is modeled within real-space real-time TDDFT using the adiabatic local density approximation (ALDA) with the param-

eterization of Perdew and Zunger[20]. Core electrons are represented by norm-conserving Troullier–Martins pseudopotentials[21]. At the first stage, the initial state of the system is prepared by performing the ground state DFT calculation. Next, the time-dependent Kohn–Sham orbitals, ψ_k, are determined by solving the equation

$$i\hbar\frac{\partial\psi_k(\mathbf{r},t)}{\partial t} = H\psi_k(\mathbf{r},t), \quad k = 1,\ldots,N_{\rm orb} \qquad (1)$$

with the Hamiltonian,

$$H = -\frac{\hbar^2}{2m}\boldsymbol{\nabla}_{\mathbf{r}} + V_{\rm H}[\rho](\mathbf{r},t) + V_{\rm XC}[\rho](\mathbf{r},t) + V_{\rm ext}(\mathbf{r},t), \quad (2)$$

where ρ is the electronic density,

$$\rho(\mathbf{r},t) = 2\sum_{k}^{N_{\rm orb}} |\psi_k(\mathbf{r},t)|^2, \qquad (3)$$

and $V_{\rm H}$ and $V_{\rm XC}$ are the Hartree and exchange-correlation potential, respectively. $V_{\rm ext}$ is the external potential, which includes the potential due to the ions, $V_{\rm ions}$, and the explicitly time-dependent potential due to the laser electric field. In the dipole approximation, $V_{\rm laser}(\mathbf{r},t) = \mathbf{r}\cdot\mathbf{E}(t)$. Assuming polarization along the x-axis, the electric field of the laser can be written as

$$\mathbf{E}(t) = \mathbf{e}_x E_{\rm max} \exp\left[-\frac{(t-\tau)^2}{2a^2}\right] \sin(\omega t). \qquad (4)$$

Here parameters a, τ, and $E_{\rm max}$ define the width, the position of the center, and the maximum electric field amplitude of the Gaussian envelope respectively, while ω is the frequency of the laser.

The time-propagation of electronic orbitals and density is achieved through the action of the time-evolution operator,

$$U(0,t) = \mathcal{T}\exp\left[-\frac{i}{\hbar}\int H(\mathbf{r},t')dt'\right], \qquad (5)$$

where $\mathcal{T}$ denotes time-ordering. In practice, the above expression for $U(t,0)$ is split into a product of multiple time-evolution operators, each corresponding to a short time step Δt,

$$U(0,t) = \prod_q U(t_q, t_q+\Delta t), \quad t_q = q\Delta t, \qquad (6)$$

so that the Hamiltonian at time t_q remains nearly commutative with the Hamiltonian at time $t_q + \Delta t$. In all calculations performed in this work we used the time step of 0.72 attoseconds, which we found to provide an acceptable balance of speed, stability, and accuracy of the time-propagation. The actual value of the time step was chosen based on our experience with other hydrocarbons subjected to laser pulses of similar intensity and duration where we monitored the conservation of the total charge (when IAP, which is discussed next, is switched off) and the convergence of the results with decreasing the time step. Also, in this work we run some test time-dependent calculations with graphene and graphane fragments subjected to a laser of zero intensity (in which case no ionization occurs) and verified the charge conservation. To represent $U(t_q, t_q+\Delta t)$ we employed the fourth order Taylor expansion,

$$\psi_k(\mathbf{r},t_q+\Delta t) \approx \sum_{n=1}^{4}\frac{1}{n!}\left(-\frac{i\Delta t}{\hbar}H(\mathbf{r},t_q)\right)^n \psi_k(\mathbf{r},t_q). \quad (7)$$

The time evolution was simulated for a period of 108 femtoseconds.

In real-space DFT and TDDFT the Kohn–Sham orbitals are represented on discrete points in real space (usually organized in uniform rectangular grids). This brings certain advantages to calculations of sophisticated electron dynamics in the case when a strong laser pulse is applied. The dynamics may involve a significant variation of the electron density within a large volume as well as ionization and fragmentation of the system. It is generally not known in advance how this process occurs. The grid representation of the orbitals allows one to describe an essentially arbitrary time-evolution, as long as the simulation cell (i.e. the area of real space covered by the numerical grids) is sufficiently large. The accuracy of such representation is easily controlled by a single parameter – the grid spacing. In our calculations we used uniform grids with x-, y-, and z-spacing of 0.25 Å.

To allow long time evolution in the calculations with real-space grids it is necessary to negate the effects of zero-boundary conditions, which causes an unphysical reflection of the wave function from the walls of the simulation cell. Given typical electron velocities and a length of the simulation cell that exceeds the system size by 5-10 Å in all directions, it only takes few femtoseconds for the electrons to reach the boundaries. This problem is traditionally solved by using an imaginary absorbing potential (IAP) or a real mask-function (a concept closely related to IAP). In our calculations we employed an imaginary absorbing potential in the form proposed by Manolopoulos[22] with an additional softening parameter to suppress extremely large IAP magnitudes at the boundaries, which can cause numerical instabilities in grid-type approaches. Since the momentum of the electrons escaping from the system lies primarily in the x-direction, the IAP in our calculations was chosen such that it only had nonzero value in the region of space next to the x-boundaries. The schematics of this set up is shown in Fig. 1. In the middle of the simulation cell, which contained the studied system (in our simulations this region ranged from x=−10 Å to 10 Å for graphene and x=−10.5 Å to 10.5 Å for graphane) the IAP is zero by definition and does not influence the system in any way. While the ponderomotive amplitude for some of the laser intensities used in our calculations well exceeded the length of the IAP-free region, our previous experience with calculations having a similar computational setup

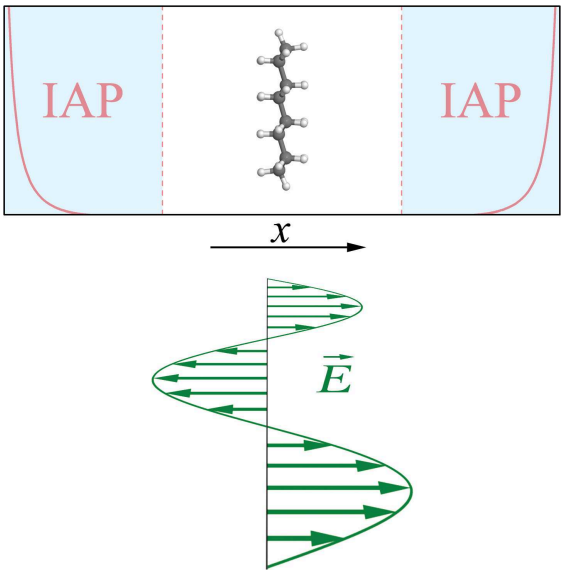

FIG. 1. (Color online) Schematic view of the simulation cell setup: the studied system is in the middle of the box, while the imaginary absorbing potential (IAP) acts in the left- and right-hand side and reaches its maximum at the walls. Laser polarization is along the x-axis.

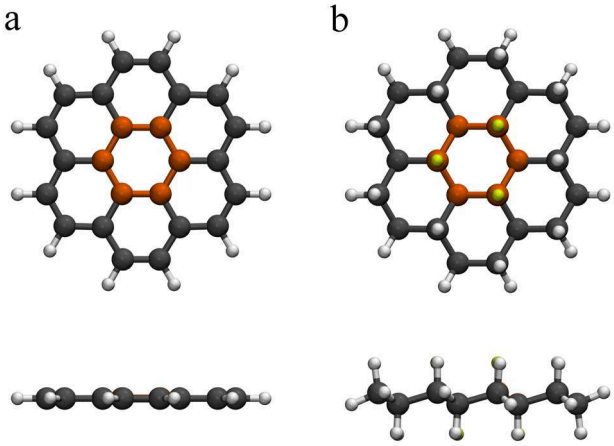

FIG. 2. (Color online) Geometric structures of the graphene (a) and graphane (b) fragments used in simulations. The ions, which were allowed to move freely during the time propagation are highlighted with orange (yellow) color.

and comparable laser pulses showed that one does not need to have an extremely large simulation cell to obtain converged results.

The ionic motion in this work is simulated by means of the Ehrenfest approach[23], in which the forces on ions are computed as the derivatives of the expectation value of the total electronic energy with respect to ionic positions, i.e.

$$M_i \frac{d^2\mathbf{R}_i}{dt^2} = \sum_{j\neq i}^{N_{\rm ions}} \frac{Z_i Z_j (\mathbf{R}_i - \mathbf{R}_j)}{|\mathbf{R}_i - \mathbf{R}_j|^3} - \boldsymbol{\nabla}_{\mathbf{R}_i} \int V_{\rm ion}(\mathbf{r}, \{\mathbf{R}\}) \rho(\mathbf{r}, t) d\mathbf{r}. \quad (8)$$

In the above classical equation of motion M_i is the mass of the i-th ion and Z_i is its pseudocharge (valence). The set of equations (8) for $i = 1 \ldots N_{\rm ions}$ is integrated simultaneously with the set of time-dependent Kohn-Sham equations (1), although the integration time step for (8) may be chosen to be somewhat longer. To integrate (8) the well known Verlet algorithm is used.

In this work, finite graphene and graphane fragments are studied. Dangling bonds at the edges of the fragments were passivated with hydrogen atoms. Most of the simulations were performed with $C_{24}H_{12}$ and $C_{24}H_{36}$ fragments shown in Fig. 2. To assess possible artifacts due to finite size, we have also repeated calculations with larger fragments in the case of graphane ($C_{37}H_{52}$). However, due to considerably higher computational cost these calculations were performed only for few selected cases. The geometric structures of the fragments were relaxed to minimize forces on ions in the absence of laser. However, the actual equilibrium positions of the carbon atoms and the hydrogens in the center of each fragment did not differ very significantly from those obtained in ground state DFT calculations with periodic boundary conditions. To preserve the general geometric features of infinite 2D systems at the time propagation stage, we fixed the positions of all ions at the edges and allowed only the ions in the middle of each fragment to move freely, as highlighted in Fig. 2. Hence, in $C_{24}H_{12}$ we had six moving carbon ions, while in $C_{24}H_{36}$ there were total of twelve (six carbons and six hydrogens) ions that could move freely. In the case of a larger graphane fragment, $C_{37}H_{52}$, the number of moving ions was equal to 26 (13 carbons and 13 hydrogens).

Note that due to the explicit time-dependence of the Hamiltonian through $V_{\rm laser}$ the total energy of the system is not constant. Therefore, the energy conservation cannot be used to assess the stability and accuracy of the calculations.

Considering the relatively short time scale of the studied phenomena any significant rearrangements of ionic positions and immediate damage to the structure can occur only if the system exhibits a strong absorption of the energy associated with the electric field. In the low intensity regime the absorption properties can be obtained from TDDFT calculations based on linear response. In this approach the system is perturbed with a weak δ-kick (which amounts to a sum of small perturbations corresponding to all possible frequencies), and then the time evolution of the dipole moment, $d(t)$, is recorded in real time[24]. The Fourier transform of $d(t) - d(0)$ taken over a sufficiently long time interval gives a good estimate of the dynamic polarizability $\alpha(\omega)$, which is related to the imaginary part of the protoabsorption cross section

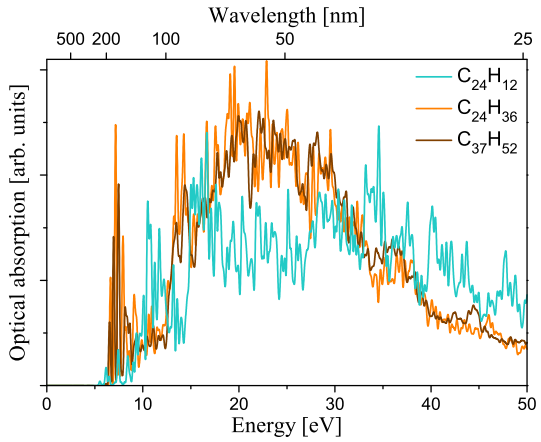

FIG. 3. (Color online) Low intensity optical absorption of graphene and graphane fragments used in this work.

through

$$\sigma(\omega) = \frac{4\pi\omega}{c}\Im\left[\alpha(\omega)\right], \tag{9}$$

where c is the speed of light. Due to the weakness of the δ-kick the induced oscillations of the dipole moment are small and essentially independent. This makes it possible to determine the strength of absorption at all frequencies in a single calculation. The optical absorption computed within the above framework can be useful for getting a rough guess of the frequency range where the system is expected to be most easily damaged. The comparison of the actual absorption properties with those predicted by Eq. (9) in some cases also serves as a good indicator of whether the system entered the nonlinear regime at a given laser intensity.

III. RESULTS AND DISCUSSION

The optical absorption spectra obtained using the linear response formalism as described above are shown in Fig. 3. In these calculations the time-propagation of the Kohn-Sham orbitals was limited to 20 fs. While the spectra themselves appear to be quite complex, the common feature for both graphene and graphane fragments is the existence of a clearly identifiable optical gap of around 6 eV. This suggests that in the low intensity regime the absorption of laser irradiation with a wavelength longer than 200 nm should be greatly suppressed.

The laser pulse duration in all calculations in this work was 35.4 fs (FWHM of intensity). In terms of the electric field amplitude such pulse has FWHM of 50 fs. The position of the Gaussian envelope peak was set at τ=54 fs.

We have performed calculations for several wavelengths ranging from the UV to IR region. We picked the values of 126, 248, 488, and 790 nm, which correspond to the wavelengths of some well known lasers, but the concrete values are of no particular importance. While the effect of the laser on the studied systems does depend on the wavelength, it does not have any pronounced resonant nature. Therefore, any other choice of wavelengths that spans a wide enough range and includes values larger and smaller than ∼200 nm would be suitable.

The maximum amplitude of the electric field in the simulations (more precisely, the maximum of the envelope function) ranged from 0 to 16 V/Å. Specifically, the following set of amplitudes were used: 0, 0.5, 1, 2, 4, 8, 12 and 16 V/Å, which in terms of laser intensity translates into 0, 3.3×10^{12}, 1.3×10^{13}, 5.3×10^{13}, 2.1×10^{14}, 8.5×10^{14}, 1.9×10^{15}, and 3.4×10^{15} W/cm^2 respectively. Given the pulse duration of 35.4 fs the energy fluence corresponding to those amplitudes is 0, 0.12, 0.5, 2, 8, 32, 72, and 128 J/cm^2.

In Fig. 4 we show the x-component of the ion displacements, $|X_i(t)-X_i(0)|$, as a function of time in a graphene fragment for three different values of the laser frequency and the maximum amplitude. In the same figure we also plot the total electron charge remaining in the system. All solid lines correspond to the calculations with zero initial temperature. While this represents only a subset of the calculations we have performed for this fragment, the basic trends can be clearly seen in Fig. 4. As expected, the data obtained for different intensities demonstrates that upon increasing the intensity of the pulse the system gets progressively more ionized. The impact of the laser also gradually becomes more pronounced when the wavelength gets smaller. What is somewhat unexpected is the fact that it takes a very strong laser ($E_{\max} \geq 8$ V/A at 126 nm) to reach the point when by the end of the simulation the graphene gets damaged, i.e. when the carbon ions are displaced considerably from their initial positions. This value of $E_{\max}$ and the corresponding fluence are larger than what we observed in similar systems (the data for graphane fragment presented below could be an example). We attribute this high strength to the planar geometric structure of graphene. While the system may be severely ionized due to the pulse, which leads to strong Coulomb repulsion between the nuclei, the net x-component of the force on ions, F_x, remains small. At the same time, F_y and F_z in an ideal planar arrangement must vanish (the system cannot expand in an infinitely large yz-plane quickly; in a finite-fragment model this is enforced by fixed atoms at the edge of the structure). Moreover, because of symmetry all ions move synchronously. Therefore, from the point of view of classical dynamics, the system of ions is in a state of unstable equilibrium. In the actual numerical calculations the symmetry is certainly not ideal (at least because of a mismatch between the hexagonal graphene structure and non-hexagonal arrangement of the grid points). Hence, the equilibrium eventually gets broken. Besides this, there is a purely physical factor that leads to breaking equilibrium in this classical picture – finite temperature. In order to investigate how significant the effect of a non-

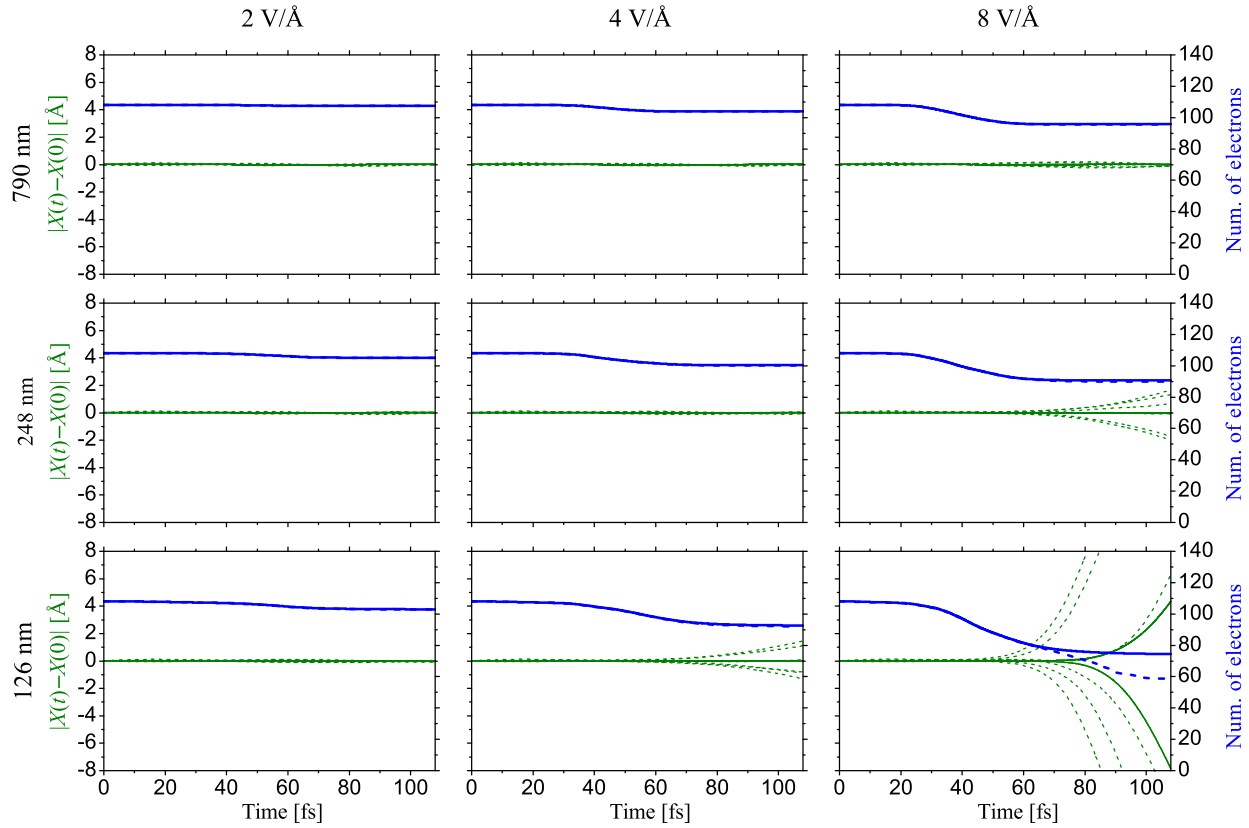

FIG. 4. (Color online) x-displacement of the carbon ions (dark green curves) as a function of time in graphene fragment subjected to 128, 248, and 790 nm laser pulses (50 fs) with a maximum amplitude ranging from 2 to 8 V/Å. The case of zero initial temperature is plotted with solid curves, while the data obtained in calculations with $T_{\rm init} = 300$ K is shown with dashed curves. The ionization of the system is plotted in parallel with blue color.

zero initial temperature on the dynamics of ions is, we carried out several calculations where in the beginning the ions were given random momenta corresponding to the Maxwell distribution at 300 K. The corresponding data is plotted in Fig. 4 with dashed lines. As can be seen in the figure, the graphene gets damaged more quickly in the case of a non-zero temperature.

The estimated single shot laser damage threshold of graphene in our simulations differs quite noticeably from the recent measurements by Roberts et al.[9], where for 50 fs 790 nm pulses the reported threshold intensity was $\sim 3\times10^{12}$ W/cm^2 ($E_{\rm max} \sim 0.5$ V/Å). In contrast, in our simulations with the 790 nm pulses and 300 K initial temperature the signs of damage began to occur at $E_{\rm max}$=12 V/Å. Part of the discrepancy comes from the longer pulse width used in the experiment. Some deficiencies of the Ehrenfest dynamics and the asymptotic form of LDA[25,26] used in the simulations may contribute as well (we believe these deficiencies should not cause qualitative changes in the ion dynamics). A more important reason for the discrepancy is likely to be the fact that the experimental conditions do not allow the use of an ideal graphene. Physical factors such as defects and adsorbates, as well as the presence of a substrate (the experiment was done on thin glass) can certainly make a significant distortion of the geometric and electronic structure and affect the stability of graphene subjected to laser irradiation. It should also be emphasized that due to computational restrictions we can only study the short-term stability (a few tens of femtoseconds after the pulse) and monitor the immediate damage to the sample. What happens to the ionized system on the longer time scale would depend on many factors, especially the environment (e.g. substrate). It is quite possible that the structural damage in graphene develops hundreds of femtoseconds or picoseconds later.

Unlike graphene, graphane does not have a single plane structure. For this reason setting the initial temperature of the ions in the simulations is not expected to have a profound effect on the dynamics of ions during a strong laser pulse. Also, on both sides of graphane there are chemical bonds with hydrogen atoms. We found that by adjusting the laser pulse intensity and, to less extent, its frequency it is possible to achieve the desorption of hydrogen ions from the surface. The general illustration of the hydrogen desorption process in graphane fragment is given in Fig. 5. As the oscillation of the electric field grows, the amplitude of the electron density oscillations

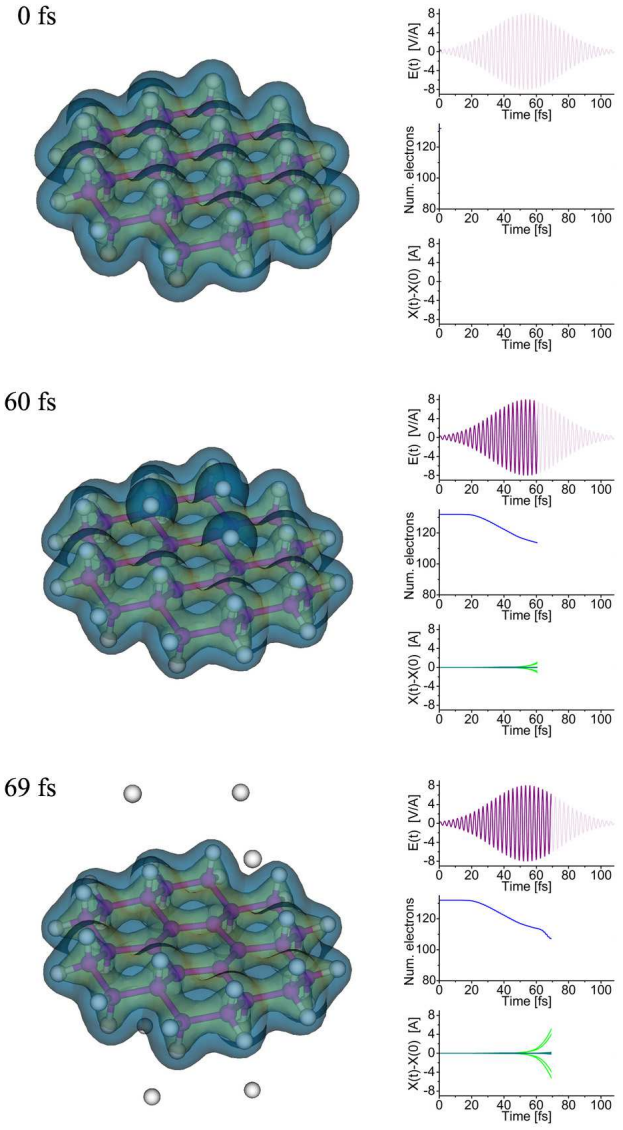

FIG. 5. (Color online) Time-evolution of the electron density and ionic positions in graphane fragment subjected to a 790nm, 35.4 fs laser pulse with the maximum electric field amplitude of 8 V/Å (enhanced online).

grows as well. Eventually, when it becomes large enough, the hydrogen ions on both sides of the surface start moving away (at that point the entire system is heavily ionized). It is interesting to note that at the initial stage of the motion, when the hydrogen ions are still close (1-4 Å) to the carbon ions they were initially attached to, the charge density around the H ions changes dramatically depending in the instantaneous direction of the electric field. Essentially, the state of the hydrogen ions oscillates between a bare proton and a hydrogen atom. These oscillations decay as the hydrogen ions move away from the surface. With each oscillation the laser continues to ionize the main target. Bare protons in close proximity (few Å) to the main target, can recapture a small fraction of the escaped electrons. However, when the direction of the electric field gets reversed, those electrons will not stay with the protons. At the time when the laser pulse is near its end the hydrogen ions are sufficiently far from the carbon surface and carry practically no electron charge with them.

A quantitative picture of the ion dynamics in the $C_{24}H_{12}$ graphane fragment is given in Fig. 6. Here, again, we present the data for three different laser frequencies and intensities. Depending on the laser parameters, three outcomes are possible. In the case of low intensities, none of the ions acquire a large enough momentum to escape. When the laser field gets stronger (for example when $E_{\max}$=8 V/Å at 790 nm) the lighter hydrogen ions begin to take off, while the motion of the heavier carbon ions exhibits only small oscillations. For such cases we also observed that the remaining six carbon atoms eventually change their structure from the initial corrugated arrangement to a planar hexagon. The ionization of the system, similar to the case of graphene, grows monotonically with intensity and it generally increases when the wavelength becomes shorter. Graphane gets ionized much more easily than graphene. In fact, for the case of $E_{\max}$=8 V/Å and 126 nm wavelength the system looses almost all its electrons during the laser pulse. Given the high degree of ionization in this case we are essentially dealing with a Coulomb explosion. The ionization is so high that even the inert carbon ions get ejected before the pulse maximum is reached. Qualitatively, the ion dynamics in this strong pulse regime is similar to the one observed in small molecules subjected to intense laser pulses and undergoing a Coulomb explosion[27].

It is interesting to comment on the kinetic energies of the ejected protons. For those combinations of laser frequency and intensity in our simulations that lead to ejection of protons, the values of the proton kinetic energies ranged approximately from 32 to 112 eV (we extrapolated our data to the limit of the infinite simulation period and cell size). The energies of individual protons in each particular simulation were very close to each other. We also observed a trend indicating that the final kinetic energy becomes saturated with the increase of the laser intensity. For example, in the case of 790 nm pulses the final kinetic energies of the ejected protons at $E_{\max}$=8,12, and 16 V/Å were 65, 95, and 112 V/Årespectively. This is another indication that the nature of the studied process is Coulomb-explosion-like. The kinetic energy cut off saturation effect is well known from the experiments on the Coulomb explosion of hydrocarbon molecules[28,29].

To verify our findings and check the adequacy of our finite-fragment models we performed a few calculations using a bigger graphane fragment, $C_{37}H_{52}$, with a larger number of freely moving ions. These calculations were only performed for the case of higher intensities when both hydrogen and carbon ions get ejected. They yielded very similar results as the calculations for the smaller fragments. In fact, the curves $|X_j(t) - X_j(0)|$ for the hydrogen ions were essentially on top of each other. The

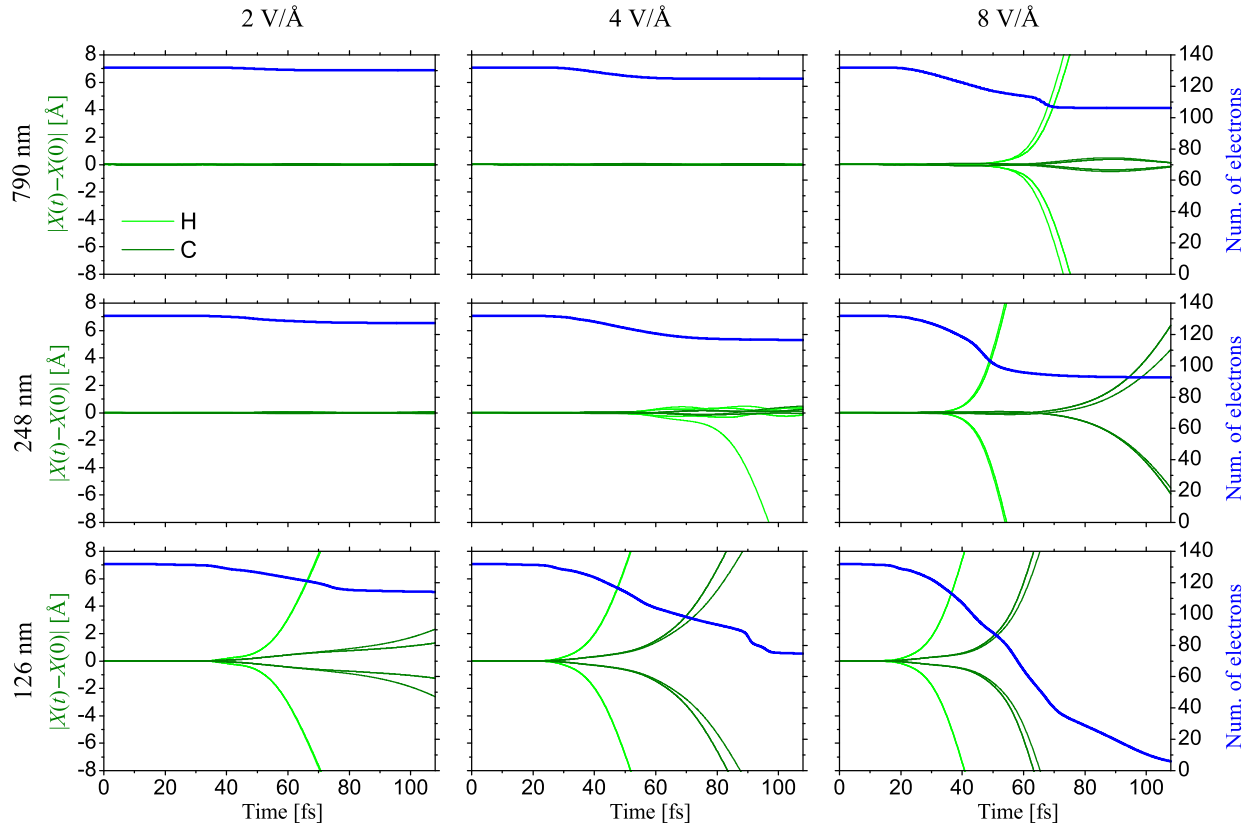

FIG. 6. (Color online) x-displacement of the hydrogen (green curves) and carbon (dark green curves) ions as a function of time in graphane fragment subjected to 128, 248, and 790 nm laser pulses (50 fs) with a maximum amplitude ranging from 2 to 8 V/Å. The ionization of the system is plotted with blue color.

curves corresponding to the displacements of carbons showed some quantitative deviation, as could be expected given the different arrangement of bonds between fixed and free carbon ions. Nonetheless, we observed a good qualitative agreement.

To summarize, in this work we have studied the response of graphene and graphane fragments to strong femtosecond laser pulses. Graphene exhibits a considerably higher immediate damage threshold due to its strictly planar structure. Finite temperature simulations that distort the planar symmetry yield structural damage at lower intensities. The survival of irradiated graphene for a time that significantly exceeds tens of femtoseconds (after the pulse) is likely to depend on experimental conditions such as laser spot size and the presence of substrate that determine its ability to quickly gain electrons from the bulk of the material to replace those lost during the laser pulse. The results obtained in the simulations of graphane demonstrate that by choosing the proper laser wavelength and intensity it is possible to achieve a desorption of hydrogen atoms without destroying the underlying layer of carbon atoms. Such a selective desorption achieved by tuning the two parameters is, in fact, a very basic realization of Quantum Optimal Control – a framework that is aimed to actively manipulate quantum dynamics using external time-dependent fields[30–34]. The effectiveness of the desorption can certainly be improved if more sophisticated pulse shapes are used.

ACKNOWLEDGMENT

This work has been supported by the National Science Foundation (grant CMMI-0927345). We also thank Prof. Arvinder Sandhu (University of Arizona) for some clarification on the experimental measurements in[9].

[1] C. W. Carr, H. B. Radousky, A. M. Rubenchik, M. D. Feit, and S. G. Demos, Phys. Rev. Lett. **92**, 087401 (2004).

[2] M. Lenzner, J. Krüger, S. Sartania, Z. Cheng, C. Spielmann, G. Mourou, W. Kautek, and F. Krausz, Phys. Rev. Lett. **80**, 4076 (1998).

[3] C.-H. Fan and J. P. Longtin, Appl. Opt. **40**, 3124 (2001).
[4] Y. L. Yao, H. Chen, and W. Zhang, Int. J. Adv. Manuf. Technol. **26**, 598 (2005).
[5] S. V. Syzranov, M. V. Fistul, and K. B. Efetov, Phys. Rev. B **78**, 045407 (2008).
[6] F. J. López-Rodríguez and G. G. Naumis, Phys. Rev. B **78**, 201406 (2008).
[7] H. L. Calvo, H. M. Pastawski, S. Roche, and L. E. F. F. Torres, Appl. Phys. Lett. **98**, 232103 (2011).
[8] M. Currie, J. D. Caldwell, F. J. Bezares, J. Robinson, T. Anderson, H. Chun, and M. Tadjer, Appl. Phys. Lett. **99**, 211909 (2011).
[9] A. Roberts, D. Cormode, C. Reynolds, T. Newhouse-Illige, B. J. LeRoy, and A. S. Sandhu, Appl. Phys. Lett. **99**, 051912 (2011).
[10] D. Wei and X. Xu, Appl. Phys. Lett. **100**, 023110 (2012).
[11] B. Krauss, T. Lohmann, D.-H. Chae, M. Haluska, K. von Klitzing, and J. H. Smet, Phys. Rev. B **79**, 165428 (2009).
[12] Y. Miyamoto, H. Zhang, and D. Tománek, Phys. Rev. Lett. **104**, 208302 (2010).
[13] H. Zhang and Y. Miyamoto, Phys. Rev. B **85**, 033402 (2012).
[14] S. Bubin and K. Varga, Appl. Phys. Lett. **98**, 154101 (2011).
[15] S. Bubin and K. Varga, J. Appl. Phys. **110**, 064905 (2011).
[16] P. Hohenberg and W. Kohn, Phys. Rev. **136**, B864 (1964).
[17] W. Kohn and L. J. Sham, Phys. Rev. **140**, A1133 (1965).
[18] E. Runge and E. K. U. Gross, Phys. Rev. Lett. **52**, 997 (1984).
[19] K. Burke, J. Werschnik, and E. K. U. Gross, J. Chem. Phys. **123**, 062206 (2005).
[20] J. P. Perdew and A. Zunger, Phys. Rev. B **23**, 5048 (1981).
[21] N. Troullier and J. L. Martins, Phys. Rev. B **43**, 1993 (1991).
[22] D. E. Manolopoulos, J. Chem. Phys. **117**, 9552 (2002).
[23] P. Ehrenfest, Z. Phys. **45**, 455 (1927).
[24] K. Yabana and G. F. Bertsch, Phys. Rev. B **54**, 4484 (1996).
[25] N. L. Doltsinis and D. Marx, J. Theor. Comput. Chem. , 319 (2002).
[26] E. Livshits and R. Baer, J. Phys. Chem. A **110**, 8443 (2006).
[27] S. Bubin, M. Atkinson, K. Varga, X. Xie, S. Roither, D. Kartashov, A. Baltuska, and M. Kitzler, (unpublished).
[28] S. Roither, X. Xie, D. Kartashov, L. Zhang, M. Schöffler, H. Xu, A. Iwasaki, T. Okino, K. Yamanouchi, A. Baltuska, and M. Kitzler, Phys. Rev. Lett. **106**, 163001 (2011).
[29] A. N. Markevitch, D. A. Romanov, S. M. Smith, and R. J. Levis, Phys. Rev. Lett. **92**, 063001 (2004).
[30] A. Assion, T. Baumert, M. Bergt, T. Brixner, B. Kiefer, V. Seyfried, M. Strehle, and G. Gerber, Science **282**, 919 (1998).
[31] M. Shapiro and P. Brumer, *Principles of Quantum Control of Molecular Processes* (Wiley, 2003).
[32] J. Werschnik and E. K. U. Gross, J. Phys. B **40**, R175 (2007).
[33] C. Brif, R. Chakrabarti, and H. Rabitz, New J. Phys. **12**, 075008 (2010).
[34] K. Krieger, A. Castro, and E. K. U. Gross, Chem. Phys. **391**, 50 (2011).